

New Photodisintegration Model of GEANT4 for the $d\gamma \rightarrow np$ Reaction with a Dibaryon Effective Field Theory

Jae Won Shin¹ and Chang Ho Hyun^{2,*}

¹*Department of Physics, Soongsil University, Seoul 156-743, Korea*

²*Department of Physics Education, Daegu University, Gyeongsan 712-714, Korea*

(Dated: 4 Aug. 2016)

Abstract

We develop a new hadronic model for GEANT4 that is specialized for the disintegration of the deuteron by photons, $d\gamma \rightarrow np$. For the description of two-nucleon interactions, we employ a pionless effective field theory with dibaryon fields (dEFT). We apply the new model of GEANT4 (G4dEFT) to the calculations of the total and the differential cross sections in $d\gamma \rightarrow np$ and compare the results with empirical data. As an application of the new model, we calculate the neutron yield from the $\gamma + \text{CD}_2$ process. G4dEFT predicts peaks for the neutron yield, but the existing model of GEANT4 does not show such behavior.

PACS numbers: 24.10.Lx, 25.20.-x, 13.60.-r

Keywords: $d\gamma \rightarrow np$, Effective field theory, Dibaryon fields, GEANT4

*Electronic address: hch@daegu.ac.kr

I. INTRODUCTION

Effective field theory (EFT) has become a popular method to study hadronic reactions with and without external probes at low energies. In the low-energy region where the scale of momenta is much smaller than the mass of pions, treating the exchange of pions, as well as heavy degrees, in terms of effective contact interactions may be reasonable. Theories thus constructed are called pionless effective field theory [1–7]. In this work, we employ a modified version of pionless theory, so-called pionless theory, with dibaryon fields (dEFT) [8]. In the dEFT, a perturbative expansion is directly manifested in physical observables such as cross-sections and their analytic forms are available.

Particle transport codes such as GEANT4 (GEometry ANd Tracking) [9, 10] are commonly utilized in the setup of plans for efficient experiments and in the analysis of results. Doing so, we can accurately estimate observables for the reactions under consideration. However, one of the authors (JWS) recently reported that built-in hadronic models of GEANT4 (v10.0) fail to describe peaks that are produced through the ${}^9\text{Be}(p,n){}^9\text{B}$ reaction in the low-energy region [11]. GEANT4 was originally built for high-energy physics. In some cases, it fails to describe low-energy phenomena correctly as was shown in the ${}^9\text{Be}(p,n){}^9\text{B}$ reaction. In Ref. 11, the authors developed a new data-based charge-exchange model for the ${}^9\text{Be}(p,n){}^9\text{B}$ reaction, and were able to achieve good agreement with experimental data.

Inspired by the observation in Ref. 11, we extend the application of GEANT4 models to low-energy processes in the two-nucleon systems. We simulate the $d\gamma \rightarrow np$ reaction by using GEANT4 code and find that an existing model of GEANT4 (v10.1) gives a null result for the total cross-section of the $d\gamma \rightarrow np$ reaction at energies below the pion threshold. In order to obtain a better description at energies below the pion threshold, we construct a dEFT-based hadronic model of GEANT4 for the $d\gamma \rightarrow np$ reaction. To check the validity of our model, we simulate the total and the differential cross-sections of the $d\gamma \rightarrow np$ process by using GEANT4 with dEFT (G4dEFT) at various energies and angles, and we compare the results with available experimental data. The result proves the usefulness of the combination of dEFT with GEANT4. As an application of the model, we calculate the neutron yields from the $\gamma + \text{CD}_2$ reaction. We find that the G4dEFT model predicts results critically different from those predicted by using existing GEANT4 models.

We organize the paper as follows; In Section II, we briefly present analytic formulae for

the differential cross-section of the dEFT, and the description of GEANT4 models relevant to this work. In Section III, we present the results for the cross sections in $d\gamma \rightarrow np$ with G4dEFT and compare them with experimental data. We propose experiments from which we can test the predictive power of G4dEFT. We summarize the work in Section IV.

II. METHODS

Large scattering lengths signal the presence of weakly-bound or almost-bound states. Through the inclusion of dibaryon fields that represent a weakly-bound state (3S_1 channel) or an almost-bound state (1S_0 channel) of two nucleons, this formulation simplifies calculations compared to the pionless theories without dibaryon fields [12–14]. We showed that the dEFT up to next-to-leading order (NLO) could be applied to diverse two-nucleon systems successfully at low energies [14–20].

The differential cross-section for the $d\gamma \rightarrow np$ reaction can be written as

$$\frac{d\sigma}{d\Omega} = \frac{\alpha}{24\pi} \frac{pE_1}{k} \sum_{\text{spin}} |A|^2, \quad (1)$$

where α is the fine structure constant, k is the energy of an incoming photon, and $E_1 = \sqrt{m_N^2 + p^2}$ is the energy of an outgoing nucleon in the center-of-mass (c.m.) frame. The spin-averaged square of the amplitude can be written as

$$\begin{aligned} S^{-1} \sum_{\text{spin}} |A|^2 &= 16(|X_{MS}|^2 + |Y_{MV}|^2) + 8(|X_{MV}|^2 + |Y_{MS}|^2) \\ &+ 12[1 - (\hat{k} \cdot \hat{p})^2](|X_E|^2 + |Y_E|^2), \end{aligned} \quad (2)$$

where S is a symmetry factor for the spin average, $S = 2$. The matrix elements X_{MV} , X_{MS} , X_E , Y_{MV} , Y_{MS} , Y_E , and the definitions of \hat{k} and \hat{p} can be found in Ref. 20.

GEANT4 (GEometry ANd Tracking) is a simulation tool kit written in the C++ language, which allows microscopic Monte Carlo simulations of the propagation of particles interacting with materials. It is being widely and successfully used in many different scientific fields, such as neutron shielding studies [21, 22], medical physics [23–25], accelerator-based radiation studies [11, 26–28], environment radiation detection studies [29–31], etc.

There are many GEANT4 physics models and cross-sections for both hadronic and electromagnetic (EM) interactions. For photonuclear interactions, however, the only GEANT4 cross-section and hadronic model relevant to this work are the

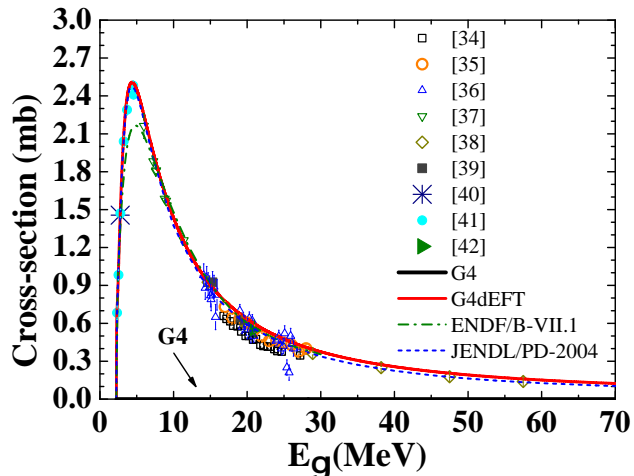


FIG. 1: (Color online) Total cross-section of the $d\gamma \rightarrow np$ reaction with respect to the incident photon energy in the laboratory frame (E_γ). Symbols denote the experimental data [34–42] taken from the EXFOR database [45]. Dot-dashed and dashed lines represent the nuclear data extracted from ENDF/B-VII.1 [43] and JENDL/PD-2004 [44], respectively. Black and red solid lines are the results obtained from G4 and G4dEFT, respectively.

“G4PhotoNuclearCrossSection” class [32] and the “G4CascadeInterface” [33] class, respectively. The G4PhotoNuclearCrossSection gives the total inelastic cross-sections for photonuclear interactions. A Bertini-style cascade model is used for G4CascadeInterface to calculate the final states of photonuclear reactions. The Bertini model is available for the incident photon energies $0 \leq E_\gamma < 3.5$ GeV in GEANT4 (v10.1), but the model has been tested mostly in the energy range $60 \text{ MeV} \sim 3 \text{ GeV}$ [33]. GEANT4 uses them by using the “G4EmExtraPhysics” GEANT4 Physics Constructor.

III. RESULTS

A. Total Cross-Section

To check the validity of GEANT4 for the $d\gamma \rightarrow np$ reaction, we first calculate the total cross-section of the reaction by using G4EmExtraPhysics (G4). In Fig. 1, we show the result of G4 as a black solid line, which is consistently zero in the energy range $E_\gamma \leq 70$ MeV. Evidently, the simulation using GEANT for the few-nucleon systems at low energies must

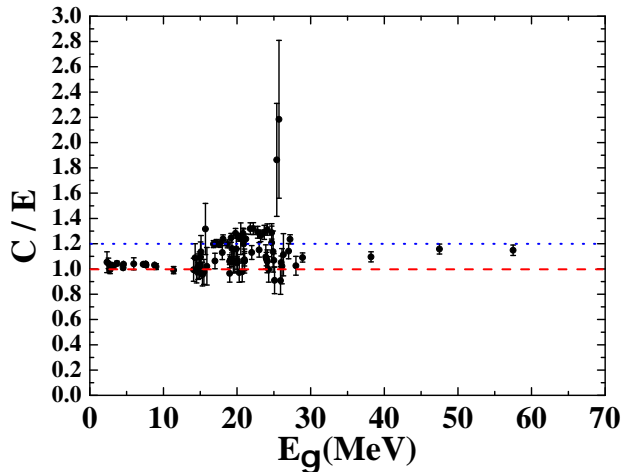


FIG. 2: Ratio of the calculated total cross-section for the $d\gamma \rightarrow np$ reaction obtained by using G4dEFT to the experimental data [34–42].

be improved. We try to incorporate the formulae of dEFT.

Figure 1 shows the total cross-section calculated by using G4dEFT (red solid line), together with the experimental data [34–42], and the evaluated nuclear data from ENDF/B-VII.1 [43] and JENDL/PD-2004 [44]. ENDF/B-VII.1 does not reproduce some experimental data around the peak, but our G4dEFT result shows good agreement with data not only around the peak, but also over the energy range considered.

The ratios of the total cross sections obtained by using G4dEFT (denoted by C) to those from experiments (denoted by E) [34–42] are shown Figure 2. The results from G4dEFT are consistent with the experimental data for the photon energy E_γ below 15 MeV within experimental errors. For the region $15 < E_\gamma < 30$ MeV, the ratios are largely located in the range from 1.0 to 1.2. There are large discrepancies (factors of ~ 2) for $E_\gamma = 25.4$ MeV and $E_\gamma = 25.7$ MeV, but experimental errors are also large. For the photon energy E_γ above 30 MeV, four experimental data are shown and agree with those from G4dEFT within about 20% error. We note that, in principle, the pionless theory will break down for momenta larger than the mass of pion. In this respect, it may make sense to compare the result with data for the photon energies below about 20 MeV. One can see that the calculated results agree well with the data in this region.

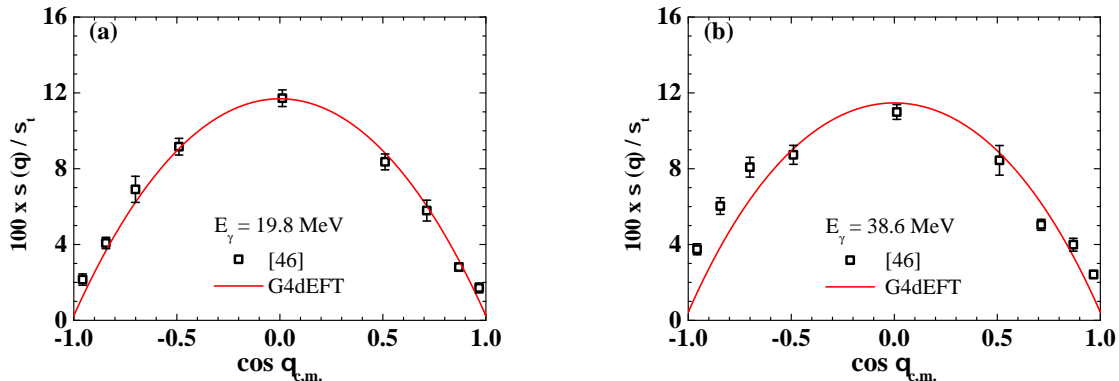


FIG. 3: (Color online) Differential cross-section $\sigma(\theta)$ as a function of $\cos\theta$ multiplied by a factor $100/\sigma_t$, where σ_t denotes the total cross-section of the unpolarized photons at the energies (a) $E_\gamma = 19.8$ MeV and (b) $E_\gamma = 38.6$ MeV. The open squares represent the experimental data taken from Ref. 46, and the solid lines denote the results obtained from G4dEFT.

B. Differential Cross-Sections

In order to investigate the quality of the model in more detail, we compare the differential cross-sections obtained from G4dEFT with the experimental data available in literature or the EXFOR database [45]. In Fig. 3, we present the differential cross-sections at photon energies (a) $E_\gamma = 19.8$ MeV and (b) $E_\gamma = 38.6$ MeV as functions of the polar angle θ in the c.m. frame. Open squares are the experimental data from Ref. 46, and solid lines represent the results of G4dEFT. For $E_\gamma = 19.8$ MeV, G4dEFT agrees with the experiment data within the error bars, but for $E_\gamma = 38.6$ MeV, there are systematic underestimates in the backward angles.

Figure 4 shows the differential cross-sections at $\theta_{\text{lab}} = 45^\circ, 75^\circ, 90^\circ$ and 105° as functions of the incident photon energy E_γ , where θ_{lab} is the polar angle in the laboratory frame. Open squares and circles represent the experimental data taken from Ref. 47 and Ref. 48, respectively. Solid lines denote the results obtained from G4dEFT. In the energy range $E_\gamma < 30$ MeV, the results of G4dEFT are mostly within the error bars regardless of the detection angles.

Some experimental works report the ratio of differential cross sections by taking $\theta_{\text{lab}} = 90^\circ$ as a reference angle [49, 50]. These works provide data sets independent of the differential cross-sections in Figs. 3 and 4. In Fig. 5, we show differential cross-sections at $\theta_{\text{lab}} = 45^\circ$,

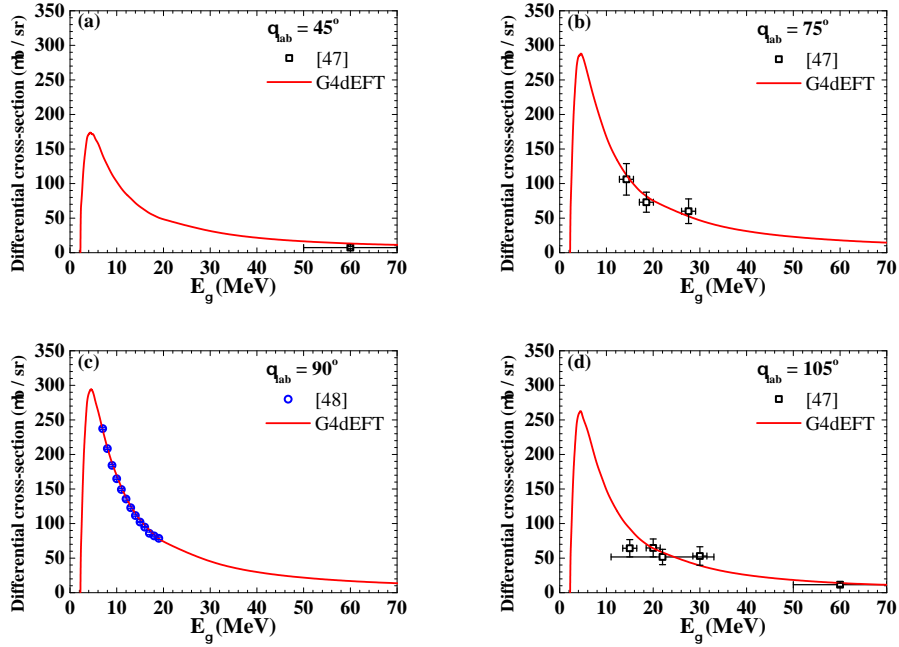


FIG. 4: (Color online) Differential cross-sections at $\theta_{\text{lab}} = 45^\circ, 75^\circ, 90^\circ$ and 105° . Open squares and circles correspond to the experimental data in Ref. 47 and Ref. 48, respectively, and the values are taken from the EXFOR database [45]. Solid lines are the results obtained from G4dEFT.

135° , and 155° divided by those at $\theta_{\text{lab}} = 90^\circ$. Experimental data are denoted with symbols, and G4dEFT results are depicted in solid lines. On the average, our results deviate from the data of Stephenson *et al.*, Ref. 49 by about 22%. Comparing the G4dEFT results to the data by Birenbaum *et al.*, Ref. 50, we have about 6% discrepancy in the energy range $7 < E_\gamma < 9$ MeV for $\theta_{\text{lab}} = 45^\circ$, but similar disagreement as that with Stephenson *et al.* appears at other angles and energies. G4dEFT cross-sections underestimate the experimental data from Ref. 50 by about 15% and 31% for $\theta_{\text{lab}} = 135^\circ$ and $\theta_{\text{lab}} = 155^\circ$ on average, respectively. On the other hand, a comparison with the data of Sawatzky [51] gives relatively good agreement at energies $E_\gamma \leq 6$ MeV. Comparison with the data of Blackston [52] shows agreement at $\theta_{\text{lab}} = 45^\circ$ with about 4.3% error, but the disagreements at $\theta_{\text{lab}} = 135^\circ$ and 155° are not resolved.

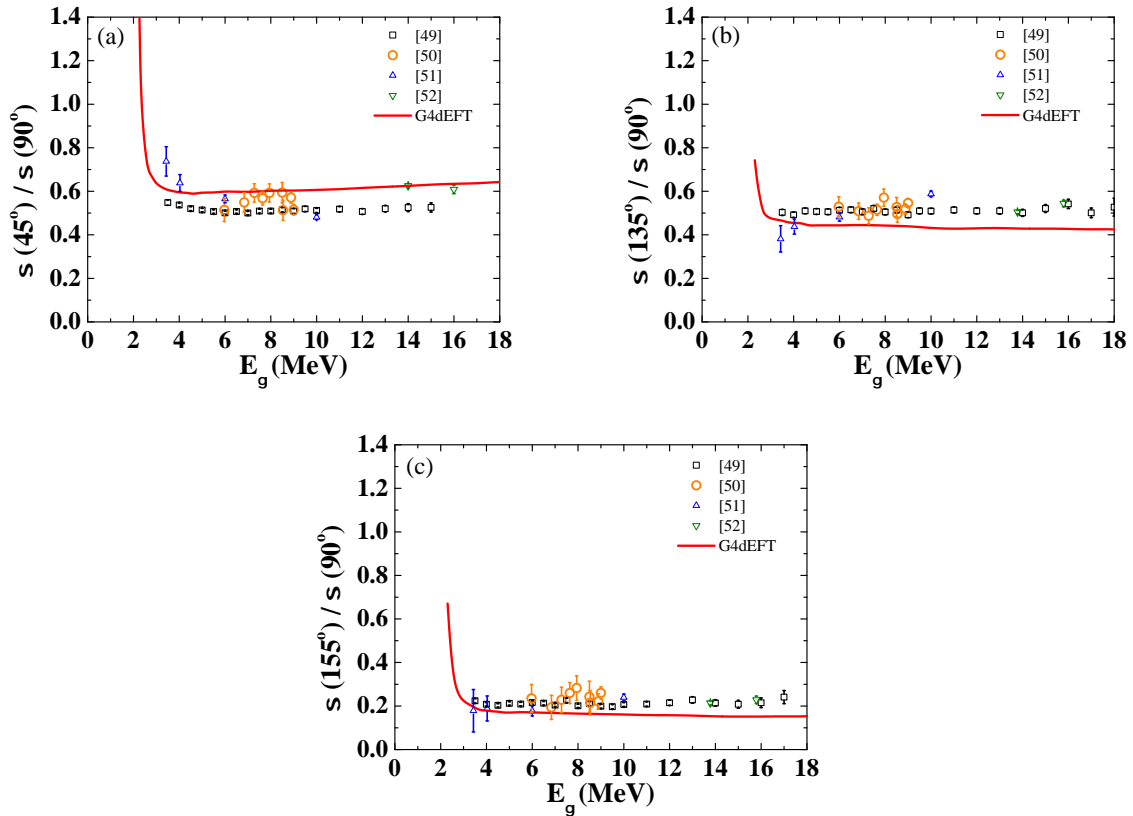


FIG. 5: (Color online) The symbols denote the experimental data in Refs. 49-52, and the actual numbers are taken from the EXFOR database [45].

C. Neutron Yields from CD_2 Photodisintegration

So far, we have focused on checking the applicability of G4dEFT by comparing our results for $d\gamma \rightarrow np$ to experimental data. As an application of G4dEFT, we attempt to predict the neutron yields from the $\gamma + \text{CD}_2$ process, which has not yet been explored either experimentally or theoretically. In this process, neutrons can be emitted from both carbon and deuteron. As shown in the $d\gamma \rightarrow np$ results in Fig. 1, different results can be anticipated from G4 and G4dEFT. One can think of gaseous (D_2) or liquid (D_2O) targets, but taking into account the advantages of the solid target, such as easy handling and large reaction rates, we chose CD_2 as a simulation material.

A schematic geometrical setup of our simulation is depicted in Fig. 6. We assume a pencil beam for the incident photons. The CD_2 target with a density of 1 g/cm^3 is modeled as a cylinder 1 cm in diameter and 1 cm in thickness. The scoring region with the shape of

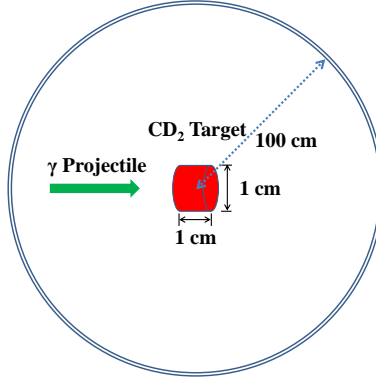


FIG. 6: (Color online) Schematic diagram of the simulation setup.

a spherical shell surrounds the target. The inner and the outer radii of the scoring region are chosen to be 100 cm and 100.1 cm, respectively. The target area is in vacuum, and the thickness of the scoring region is chosen as 0.1 cm arbitrarily for convenience and does not affect the results.

For the EM processes and hadronic interactions of hadrons in our simulations, we use GEANT4 physics lists, “G4EmLivermorePhysics” and “G4HadronPhysicsQGSP_BIC_HP” classes, respectively.¹ As mentioned in Sec. II, GEANT4 uses G4EmExtraPhysics for photonuclear interactions. G4EmExtraPhysics can be applied to carbon materials, but as we have shown, it is not valid for the deuteron in the low-energy region. To see the effect of the deuteron, we simulate the $\gamma + \text{CD}_2$ process by considering two cases. One is the case using only G4EmExtraPhysics (G4), and the other is the case using both G4EmExtraPhysics and G4dEFT (G4 + G4dEFT).

Figure 7 shows the distribution of neutrons scored in the shell as a function of the neutron energy E_n for (a) $E_\gamma = 9.8$ MeV, and (b) $E_\gamma = 19.8$ MeV. In each plot, the results of G4 (G4+G4dEFT) are denoted as filled circles (open squares). Let us analyze the results of G4 first. As shown in Fig. 1, the cross section of $d\gamma \rightarrow np$ is null in G4, so the neutrons for G4 in Fig. 7 are emitted only from carbon nuclei in CD_2 . For $E_\gamma = 9.8$ MeV, very small

¹ There are many different pre-defined physics constructors in GEANT4. To check the dependence on the constructors, we simulated both the photon flux in the CD_2 target and the neutron yields generated by $d\gamma \rightarrow np$ reaction with different GEANT4 physics constructors, separately, but the differences due to the constructors were almost negligible because the simulated observables discussed in this work came from the $d\gamma \rightarrow np$ reaction by using G4dEFT.

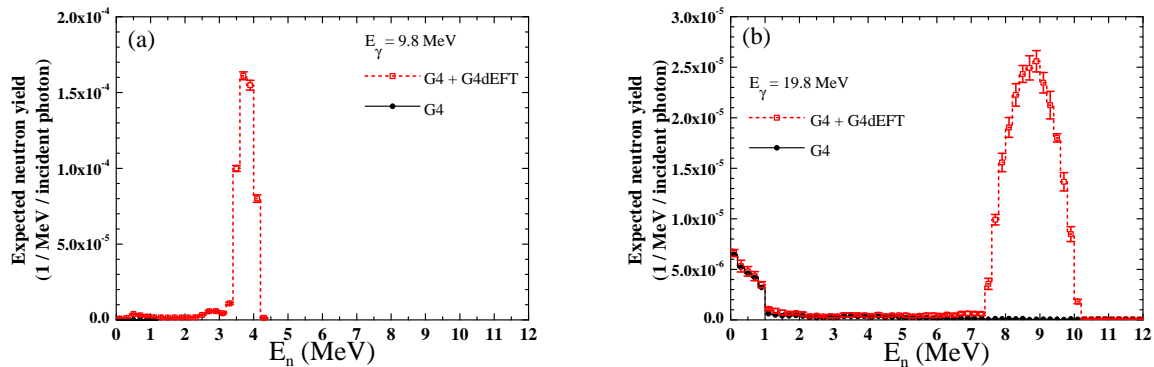


FIG. 7: (Color online) Expected energy spectra of neutron yields due to photons of energies (a) 9.8 MeV and (b) 19.8 MeV incident on a CD_2 target. The black solid line with filled circles and the red dotted line with open squares represent the results obtained by using GEANT4 with G4 and G4 + G4dEFT, respectively.

numbers of neutrons are emitted up to $E_n \sim 1$ MeV, but more energetic neutrons are not produced. In the target, we assume natural carbon, $^{\text{nat}}\text{C}$, in which about 99% is ^{12}C , and the remaining 1% is mostly ^{13}C . The threshold for the $^{12}\text{C}(\gamma, n)$ reaction is 18.737 MeV, so the black circles in Fig. 7 (a) denote the neutrons emitted from ^{13}C only. Because the fraction of ^{13}C is very small in nature, the production of neutrons is also very small. Due to energy conservation, the maximum energy of the emitted neutrons is limited. This is the reason the neutron production is truncated at $E_n \sim 1$ MeV. For $E_\gamma = 19.8$ MeV, the photon energy exceeds the threshold of the $^{12}\text{C}(\gamma, n)$ reaction, so we have a substantial number of neutrons in the energy range $E_n = 0 \sim 1$ MeV. The number of neutrons drops abruptly around $E_n \sim 1$ MeV, which is also due to the conservation of the energy of the neutrons emitted from ^{12}C . The black circles indicate the number of neutrons emitted from ^{13}C at energies above $E_n \sim 1$ MeV. Here again, the small numbers in the range $E_n \geq 1$ MeV reflect the small fraction of ^{13}C in nature.

Now, let us discuss the results of G4+G4dEFT. In this model, the neutrons are contributed by both carbon and deuteron. The neutron yield in the G4+G4dEFT model is similar to that in the G4 model in the ranges $E_n \leq 1$ MeV for $E_\gamma = 9.8$ MeV and $E_n \leq 7.4$ MeV for $E_\gamma = 19.8$ MeV. However, significant differences occur around $E_n \sim 3.7$ MeV for $E_\gamma = 9.8$ MeV and around $E_n \sim 8.7$ MeV for $E_\gamma = 19.8$ MeV, where high and broad peaks

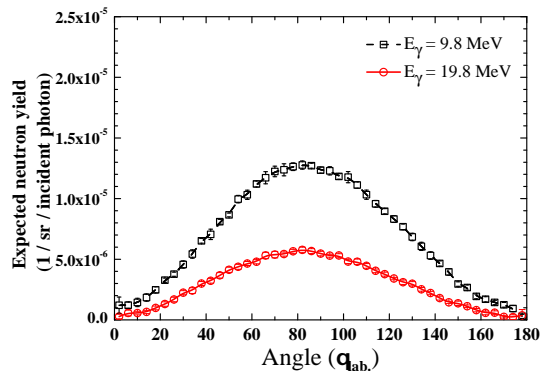


FIG. 8: (Color online) Expected angular distributions of neutron yields in the G4+G4dEFT model. The black dotted line with squares and the red solid line with circles represent the results for 9.8 MeV and 19.8 MeV photons, respectively.

appear. The number of neutrons produced by the $d\gamma \rightarrow np$ reaction is obtained by making use of the “G4UserSteppingAction” class. The ratio of the neutron number for $E_\gamma = 9.8$ MeV to that for $E_\gamma = 19.8$ MeV is obtained as 2.293 ± 0.046 . This number is close to the ratio of the total cross-sections of the $d\gamma \rightarrow np$ process, 2.287, for $E_\gamma = 9.8$ MeV (1.44 mb) and for $E_\gamma = 19.8$ MeV (0.63 mb). The similarity of two ratios is proof that the peaks in Fig. 7 originate from interactions of photons and deuterons.

In Fig. 8, we show the angular distribution of the neutron yield. The maximum values are located around $\theta_{\text{lab}} = 90^\circ$, which is in agreement with the behavior of the differential cross-section of the $d\gamma \rightarrow np$ process, Fig. 3. This coincidence proves again that most of the neutrons in the peaks are emitted from the deuterons in CD_2 . The angular distribution for $E_\gamma = 19.8$ MeV is relatively broader than that for $E_\gamma = 9.8$ MeV, which is one of the reasons we have a peak broader for $E_\gamma = 19.8$ MeV than for $E_\gamma = 9.8$ MeV in Fig. 7.

The distribution of the emitted neutrons in terms of the energy at $\theta_{\text{lab}} = 90^\circ$ is plotted in Fig. 9. Very sharp peaks are seen at $E_n \sim 3.7$ MeV for $E_\gamma = 9.8$ MeV and at $E_n \sim 8.7$ MeV for $E_\gamma = 19.8$ MeV. If one treats the scattering process $d\gamma \rightarrow np$ classically and calculates the energy of outgoing neutrons in the laboratory frame, one can easily obtain $E_n = 3.7$ MeV and 8.7 MeV for $E_\gamma = 9.8$ MeV and 19.8 MeV, respectively. The coincidence of these values and the positions of the peaks signal the dominance of $d\gamma$ reactions in the emission of neutrons.

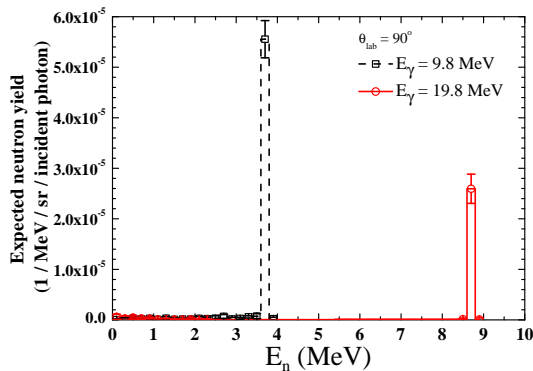


FIG. 9: (Color online) Expected neutron energy spectra at $\theta_{\text{lab}} = 90^\circ$ produced by photons on a CD_2 target in the G4+G4dEFT model.

IV. SUMMARY

With the development of effective field theories in nuclear physics, the accuracy in describing and understanding few-nucleon systems is being improved unprecedentedly. The improvement will make it possible to have more precise results for simulations in which few-nucleon processes will contribute non-negligibly. Our work started from the question of how we could embed the progress of nuclear theory for few-nucleon systems in the simulations of nuclear processes. As a first step, we checked the validity of G4EmExtraPhysics, which accounts for the photonuclear interactions in GEANT4 (v10.1) by calculating the total cross-section of the $d\gamma \rightarrow np$ process. We found that the G4EmExtraPhysics model gave null result for the total cross-section of the process at energies below the pion threshold. In order to resolve the problem and enhance the predictive power of simulations, we incorporated analytic results of a dibaryon effective field theory into GEANT4.

The new model has been checked thoroughly by calculating the total and the differential cross-sections of the $d\gamma \rightarrow np$ process for incident photon energies up to 70 MeV and by comparing the results with available experimental data. G4dEFT gives results within the experimental error bars for E_γ below 15 MeV. For photon energies above 15 MeV, the results from G4dEFT show reasonable agreement with those from experiments within 20%, even though the energy region is out of the valid range for the theory.

The model has been applied to calculate the yield of neutrons emitted from CD_2 bombarded by photons. Because no experimental datum is available for the observable, only a

comparison between the new and the existing models was made. The two models show a critical difference in the prediction of the neutron yield. The measurement, if performed, will provide criteria about the accuracy and the extent to which the model is valid and applicable.

Acknowledgments

This research was supported by the Daegu University Research Grant, 2013.

-
- [1] D. B. Kaplan, M. J. Savage, and M. B. Wise, Nucl. Phys. B **478**, 629 (1996).
 - [2] J. W. Chen, G. Rupak, and M. J. Savage, Nucl. Phys. A **653**, 386 (1999).
 - [3] J. W. Chen, G. Rupak, and M. J. Savage, Phys. Lett. B **464**, 1 (1999).
 - [4] J. W. Chen and M. J. Savage, Phys. Rev. C **60**, 065205 (1999).
 - [5] G. Rupak, Nucl. Phys. A **678**, 405 (2000).
 - [6] S. R. Beane, and M. J. Savage, Nucl. Phys. A **694**, 511 (2001).
 - [7] H. W. Griesshammer, and G. Rupak, Phys. Lett. B **529**, 57 (2002).
 - [8] D. B. Kaplan, Nucl. Phys. B **494**, 471 (1997).
 - [9] S. Agostinelli *et al.*, Nucl. Instrum. Meth. A **506**, 250 (2003).
 - [10] J. Allison *et al.*, IEEE Trans. Nucl. Sci. **53**, 270 (2006).
 - [11] J. W. Shin and T.-S. Park, Nucl. Instrum. Meth. B **342**, 194 (2015).
 - [12] P. F. Bedaque, and U. van Kolck, Phys. Lett. B **428**, 221 (1998).
 - [13] U. van Kolck, Nucl. Phys. A **645**, 273 (1999).
 - [14] S. Ando, and C. H. Hyun, Phys. Rev. C **72**, 014008 (2005).
 - [15] S. Ando, R. H. Cyburt, S. W. Hong, and C. H. Hyun, Phys. Rev. C **74**, 025809 (2006).
 - [16] S. Ando, J. W. Shin, C. H. Hyun, and S. W. Hong, Phys. Rev. C **76**, 064001 (2007).
 - [17] S. Ando, J. W. Shin, C. H. Hyun, S. W. Hong, and K. Kubodera, Phys. Lett. B **668**, 187 (2008).
 - [18] J. W. Shin, S. Ando, and C. H. Hyun, Phys. Rev. C **81**, 055501 (2010).
 - [19] J. W. Shin, S.-I. Ando, C. H. Hyun, and S. W. Hong, Few-Body Syst. **54**, 359 (2013).
 - [20] J. W. Shin, C. H. Hyun, S.-I. Ando, and S. W. Hong, Phys. Rev. C **88**, 035501 (2013).

- [21] S. I. Bak, T. S. Park, S. W. Hong, J. W. Shin, and I. S. Hahn, *J. Korean Phys. Soc.* **59**, 2071 (2011).
- [22] J. W. Shin, S. W. Hong, S.-I. Bak, D. Y. Kim, and C. Y. Kim, *J. Korean Phys. Soc.* **65**, 591 (2014).
- [23] M. U. Bug, E. Gargioni, S. Guatelli, S. Incerti, H. Rabus, R. Schulte, and A. B. Rosenfeld, *Eur. Phys. J. D* **60**, 85 (2010).
- [24] J. W. Shin, S. W. Hong, C. I. Lee, and T. S. Suh, *J. Korean Phys. Soc.* **59**, 12 (2011).
- [25] C. I. Lee, J. W. Shin, S.-C. Yoon, T. S. Suh, S.-W. Hong, K. J. Min, S. D. Lee, S. M. Chung, and J.-Y. Jung, *J. Korean Phys. Soc.* **66**, 1308 (2015).
- [26] J. K. Park, S. Kwon, S. W. Lee, J. T. Kim, J.-S. Chai, J. W. Shin, and S.-W. Hong, *J. Korean Phys. Soc.* **58**, 1511 (2011).
- [27] J. W. Shin, T.-S. Park, S. W. Hong, J. K. Park, J. T. Kim, and J.-S. Chai, *J. Korean Phys. Soc.* **59**, 2022 (2011).
- [28] J. W. Shin *et al.*, *Nucl. Instrum. Meth. A* **797**, 304 (2015).
- [29] S. Hurtado, M. García-León, and R. García-Tenorio, *Nucl. Instrum. Meth. A* **518**, 764 (2004).
- [30] K. Banerjee *et al.*, *Nucl. Instrum. Meth. A* **608**, 440 (2009).
- [31] P. M. Joshirao, J. W. Shin, C. K. Vyas, A. D. Kulkarni, H. Kim, T. Kim, S.-W. Hong, and V. K. Manchanda, *Appl. Radiat. Isot.* **81**, 184 (2013).
- [32] J. P. Wellisch, M. Kossov, and P. Degtyarenko, arXiv:nucl-th/0306012.
- [33] A. Heikkinen, N. Stepanov, and J. P. Wellisch, arXiv:nucl-th/0306008.
- [34] J. E. E. Baglin, R. W. Carr, E. J. Bentz, and C.-P. Wu, *Nucl. Phys. A* **201**, 593 (1973).
- [35] D. M. Skopik, Y. M. Shin, M. C. Phenneger, and J. J. Murphy, *Phys. Rev. C* **9**, 531 (1974).
- [36] J. Ahrens, H. B. Eppler, H. Gimm, M. Kröning, P. Riehn, H. Wäffler, A. Zieger, and B. Ziegler, *Phys. Lett. B* **52**, 49 (1974).
- [37] Y. Birenbaum, S. Kahane, and R. Moreh, *Phys. Rev. C* **32**, 1825 (1985).
- [38] R. Bernabei *et al.*, *Phys. Rev. Lett.* **57**, 1542 (1986).
- [39] R. Bernabei *et al.*, *Phys. Rev. C* **38**, 1990 (1988).
- [40] R. Moreh, T. J. Kennett, and W. V. Prestwich, *Phys. Rev. C* **39**, 1247 (1989).
- [41] K. Y. Hara *et al.*, *Phys. Rev. D* **68**, 072001 (2003).
- [42] T. Shima, S. Naito, Y. Nagai, T. Baba, K. Tamura, T. Takahashi, T. Kii, H. Ohgaki, and H. Toyokawa, *Phys. Rev. C* **72**, 044004 (2005).

- [43] <http://www.nndc.bnl.gov/csewg/>.
- [44] <http://wwwndc.jaea.go.jp/ftpnd/jendl/jendl-pd-2004.html>.
- [45] <https://www-nds.iaea.org/exfor/exfor.htm>.
- [46] M. P. De Pascale *et al.*, Phys. Rev. C **32**, 1830 (1985).
- [47] I. Akkurt, Chin. J. Phys. **41**, 111 (2003).
- [48] A. De Graeve, A. Zieger, R. Van De Vyver, C. Van Den Abeele, H. Ferdinande, L. Van Hoorebeke, D. Ryckbosch, F. De Smet, and B. Ziegler, Nucl. Phys. A **530**, 420 (1991).
- [49] K. E. Stephenson, R. J. Holt, R. D. Mckeown, and J. R. Specht, Phys. Rev. C **35**, 2023 (1987).
- [50] Y. Birenbaum, Z. Berant, A. Wolf, S. Kahane, and R. Moreh, Phy. Rev. Lett. **61**, 810 (1988).
- [51] B. Sawatzky, Ph.D. thesis, University of Virginia, 2005.
- [52] M. Blackston, Ph.D. thesis, Duke University, 2007.